

THE RØMER DELAY AND MASS RATIO OF THE SDB+DM BINARY 2M 1938+4603 FROM *KEPLER* ECLIPSE TIMINGS

BRAD N. BARLOW, RICHARD A. WADE, AND SANDRA E. LISS

Department of Astronomy and Astrophysics, 525 Davey Lab, The Pennsylvania State University, University Park, PA 16802, USA

Accepted for publication in The Astrophysical Journal

ABSTRACT

The eclipsing binary system 2M 1938+4603 consists of a pulsating hot subdwarf B star and a cool M dwarf companion in an effectively circular three-hour orbit. The light curve shows both primary and secondary eclipses, along with a strong reflection effect from the cool companion. Here we present constraints on the component masses and eccentricity derived from the Rømer delay of the secondary eclipse. Using six months of publicly-available *Kepler* photometry obtained in Short Cadence mode, we fit model profiles to the primary and secondary eclipses to measure their centroid values. We find that the secondary eclipse arrives on average 2.06 ± 0.12 s after the midpoint between primary eclipses. Under the assumption of a circular orbit, we calculate from this time delay a mass ratio of $q = 0.2691 \pm 0.0018$ and individual masses of $M_{\text{sdb}} = 0.372 \pm 0.024 M_{\odot}$ and $M_c = 0.1002 \pm 0.0065 M_{\odot}$ for the sdB and M dwarf, respectively. These results differ slightly from those of a previously-published light curve modeling solution; this difference, however, may be reconciled with a very small eccentricity, $e \cos \omega \approx 0.00004$. We also report an orbital period decrease of $\dot{P} = (-1.23 \pm 0.07) \times 10^{-10}$.

Subject headings: binaries: close — binaries: eclipsing — subdwarfs — techniques: photometric — stars: 2M 1938+4603

1. INTRODUCTION

Around ten eclipsing hot subdwarf B (sdB) star binaries are known presently (e.g., For et al. 2010); they have orbital periods from 2-4 hours, and the companions are typically low-mass M dwarfs. Although these subdwarfs outshine their companions at all visible (and most infrared) wavelengths, the high albedo of the M dwarf and its large subtended solid angle as seen from the sdB star lead to a strong reflection effect, and, consequently, these systems exhibit both primary eclipses (when the M dwarf transits the sdB) and secondary eclipses (when the sdB blocks reflected light from the M dwarf). Binary population synthesis (BPS) models (e.g., Han et al. 2002, 2003; Clausen et al. 2012) show they are likely a product of a past common-envelope (CE) stage during which the sdB progenitor filled its Roche lobe while on the red giant branch and lost most of its outer H envelope. Assessing the distribution of their orbital parameters and masses can test binary evolution scenarios and help constrain the parameterizations in BPS codes. Masses have been derived from light-curve modeling solutions for the majority of known detached sdB+dM systems (e.g., For et al. 2010), but the accuracy of these results has not been tested thoroughly using independent techniques.

Precise measurements of the eclipse timings in sdB+dM binaries provide an opportunity to measure the component masses in a relatively model-independent way. An observer watching one of these systems face-on from a great distance would see a syzygy of the sdB, its companion, and Earth every half orbital period, if the orbit is circular. An observer on Earth, however, has a different experience. Since the mass ratio does not equal unity, the primary and secondary stars will occult the light from the other star while at different displacements from the binary center of mass. That is, the eclipses as seen from Earth emanate from different line-of-sight

distances. The secondary eclipses will arrive *later than* the halfway point between primary eclipses. (Here we use “primary eclipse” to refer to the eclipse of the primary star, assumed to be brighter and more massive.) Using measurements of the orbital period, the sdB velocity semi-amplitude, the inclination angle, and the time delay (Rømer delay) of the secondary eclipse, one can determine both masses, as if the system were a double-lined spectroscopic binary (Kaplan 2010). The method is applicable to eccentric systems, too, but the orbital geometry must be determined first since eccentricity shifts the relative timing of the two eclipses.

2M 1938+4603, or KIC 9472174 (hereafter, 2M 1938¹), is a bright ($g=11.96$) eclipsing sdB+dM binary that lies in the *Kepler* field and a suitable test case for the technique described above. The system exhibits grazing primary and secondary eclipses along with a strong reflection effect from the cool secondary (Østensen et al. 2010, hereafter Ø10); the period is 3.0 h, and the orbit appears to be nearly circular. The analysis described by Kaplan (2010) predicts the secondary eclipse should occur 2.35 ± 0.10 s after the midpoint between primary eclipses, assuming the mass ratio from Ø10’s light curve modeling solution, $q=0.244 \pm 0.008$. This time delay should be observable given sufficient measurements. After phase-folding a nine day long light curve obtained from *Kepler* during quarter 0 (Q0) of operations, Ø10 found evidence for more than 55 pulsational frequencies covering both the p- and g-mode domains in frequency space. Although the amplitudes are quite small ($< 0.1\%$), the rich pulsation spectrum might permit asteroseismic models to establish the mass of the sdB. Thus 2M 1938 offers an opportunity to compare mass determinations for an sdB star, obtained by different methods.

Here we present an analysis of more than six months

¹ The full 2MASS designation is 2MASS J19383260+4603591.

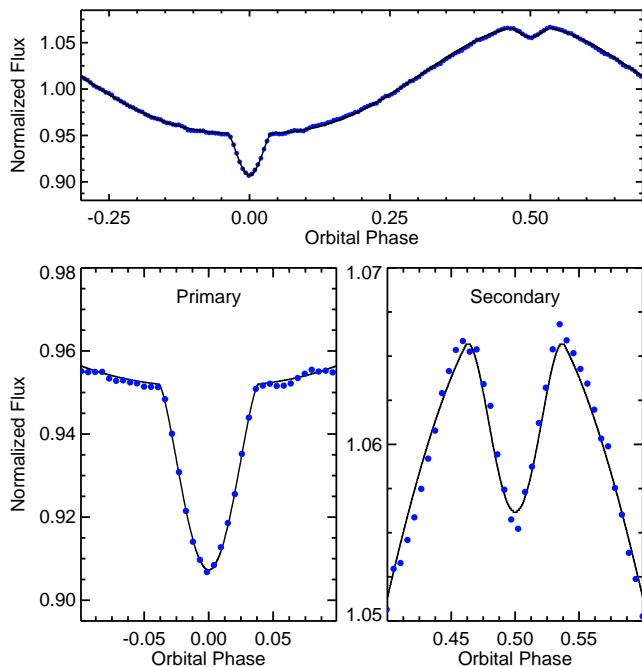


FIG. 1.— **Top panel:** Our best-fitting light curve model from BINARY MAKER 3.0 (solid black line) plotted on top of a randomly-selected cycle in the *Kepler* light curve (blue points). The secondary eclipse observed during this cycle happens to be particularly affected by the constructive interference of pulsations and chunking (see text). The average photometric accuracy in each point is around 0.04%. **Bottom panels:** Enlarged portions of the top panel showing the primary eclipse (left) and secondary eclipse (right) profiles. The poor sampling across the eclipses combined with chunking and the pulsations leads to an asymmetry in the observed profiles that varies from cycle to cycle.

of short-cadence *Kepler* photometry taken during Q0, quarter 5 (Q5) and quarter 6 (Q6) of operations. Our primary goal was to measure the secondary time delay. Using fits to the eclipse profiles we confirm that there is a time delay, which we use in combination with data from Ø10 to compute masses for the sdB and M dwarf. We compare our results with the light-curve modeling solution of Ø10.

2. OBSERVATIONS

In May 2009 and from March 2010 to September 2010, *Kepler* observed 1436 orbital cycles of 2M 1938 using short-cadence observations. In this operating mode, nine 6.02-s exposures, each with a readout time of 0.52 s, are summed into memory to produce an image every 58.85 s (92% duty cycle). We downloaded the public Q0, Q5 and Q6 light curves from the *Kepler* data archive². We converted the time stamps, given as Barycentric *Kepler* Julian Date and accurate to ± 0.05 s, to Barycentric Julian Date. Gilliland et al. (2010) give additional characteristics of *Kepler* short-cadence data.

3. MEASURING THE RØMER DELAY

We constructed a model light curve to use as a template for fitting each eclipse, using BINARY MAKER 3.0³

² <http://archive.stsci.edu/kepler>

³ <http://www.binarymaker.com/>

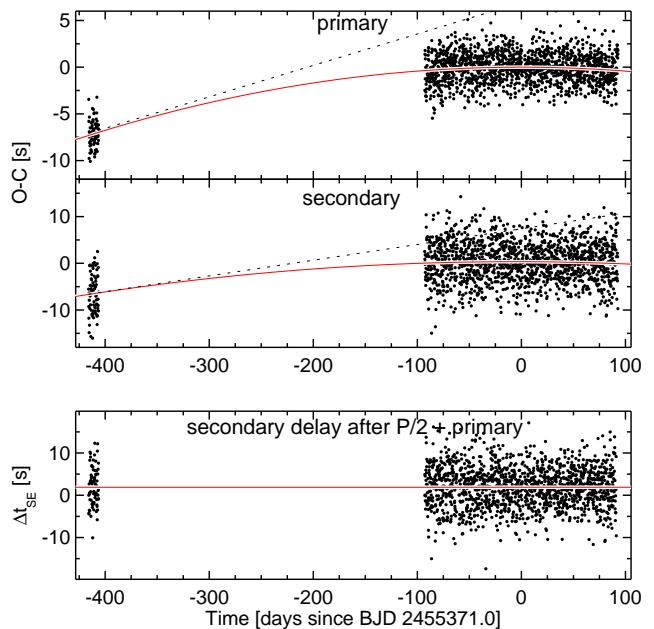


FIG. 2.— **Top panels:** Primary and secondary eclipse O-C diagrams (not on the same scale) from the Q0, Q5, and Q6 *Kepler* light curves. Both plots show evidence of a period decrease. The dotted line represents Ø10's linear ephemeris from Q0, while the solid line shows our quadratic ephemeris. **Bottom panel:** Time delay of the secondary eclipse with respect to one half period after the primary eclipse, which does not significantly change from Q0 to Q5/Q6. The mean Δt_{SE} is shown by a solid horizontal line.

with the orbital parameters reported by Ø10⁴. As shown in Figure 1, the model reproduces the observations reasonably well. We cross-correlated the primary and secondary eclipse template profiles against each observed eclipse to determine the times of minima. The model was re-sampled step-by-step as it was swept across each eclipse to match the sampling of the observations. Since finite integration times introduce asymmetric distortions to the eclipse profiles (see Kipping 2010), we attempted to emulate the exposure times by integrating each sampling point in a similar manner as the *Kepler* data to better match the observed profiles. Before the correlations were made, each eclipse and its surrounding continuum were cropped from the light curves and normalized by polynomial fits to the continuum. The same fit was used for every model-observation pair. We note that we do not fit the eclipse depths or durations in this work; only times of minima are reported. We also investigated the effects of both orbital (Shakura & Postnov 1987) and rotational (Groot 2012) Doppler boosting, which asymmetrically skew the eclipse profiles, but found only negligible changes in the fit parameters for the expected levels of boosting in this system.

Tables 1 and 2 (online) present the measured eclipse times, which have an average uncertainty of a few seconds. Using the linear orbital ephemeris given by Ø10 as a starting point, we constructed two *observed minus calculated* (O-C) diagrams, one for the primary eclipse and another for the secondary. These are shown in Figure 2 and reveal a seven-second phase shift between Q0 and

⁴ Ø10 do not cite a secondary bolometric albedo; we used $A_2=1.2$.

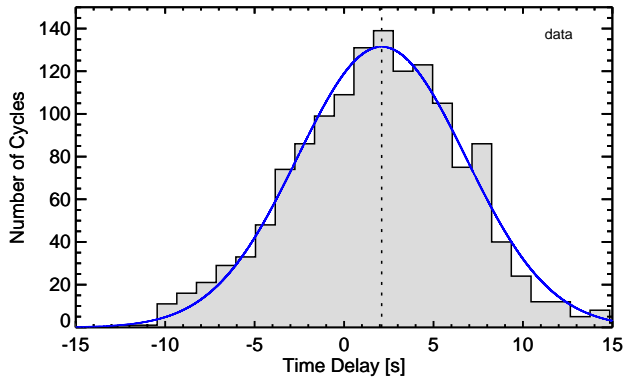


FIG. 3.— Histogram of the secondary eclipse time delays, measured with respect to the mid-point between primary eclipses. Data represent 1493 pairs of primary and secondary eclipses obtained in Q0, Q5, and Q6. The Gaussian (solid line) that best fits the distribution is centered at 2.06 ± 0.12 s.

the beginning of Q5; the data cannot be fitted well with a linear ephemeris. From a parabolic fit to all three quarters, we report an ephemeris for primary eclipses defined by

$$\begin{aligned} T_o &= 2455\,369.422\,466\,9 \pm 0.000\,000\,5 \text{ BJD} \\ P &= 0.125\,765\,251 \pm 0.000\,000\,002 \text{ days} \\ \dot{P} &= (-1.23 \pm 0.07) \times 10^{-10} \end{aligned}$$

The zero-point was chosen to be near the transition time between Q5 and Q6. Fits to the secondary eclipse O-C diagram (middle panel of Figure 2) give consistent results for the period and its first derivative, which corresponds to a nearly 4 ms decrease in the orbital period each year. The derived period during Q5/Q6 does not agree with the Q0 result of Ø10, but this is due to the non-zero \dot{P} , which was unknown at the time. Using our updated ephemeris to derive the period during Q0, we find the same value they do. Orbital decays have been observed for other sdB+dM systems (e.g., Qian et al. 2012) and might be explained by tidal dissipation, magnetic braking, and gravitational wave emission; the latter effect, however, predicts a period change several orders of magnitude slower than what we observe for 2M 1938. We note that a long-period sinusoidal oscillation in the O-C diagram could mimic a \dot{P} ; only additional measurements over an extended baseline will help discriminate between these possibilities.

As mentioned above, we do not expect the secondary eclipse to occur exactly halfway between primary eclipses since the mass ratio given by Ø10 is far from unity. In the bottom panel of Figure 2, we plot deviations of the secondary eclipse times from $1/2$ period after the primary eclipses (hereafter, Δt_{SE}). Even with the large spread in Δt_{SE} values, the mean is visibly offset from zero. The offset becomes clearer in a histogram of the measured time delays, as shown in Figure 3. A Gaussian centered at 2.06 ± 0.12 s with a full width half maximum (FWHM) of 11 s fits the distribution well. Its centroid agrees with the mean of all Δt_{SE} values, 1.88 ± 0.13 s. *Indeed, the secondary eclipse lags behind the mid point between primary eclipses, by approximately two seconds.*

Before proceeding, we computed the Fourier transforms (FTs) of the O-C and Δt_{SE} curves to identify and

analyze any periodic signals that might be present. Only Q5 and Q6 were considered in this exercise since the addition of Q0 and the gap it introduces complicates the window function. The upper panels of Figure 4 present the O-C diagrams next to their amplitude spectra, which are plotted out to the Nyquist frequency ($3.976 \text{ day}^{-1} = 1/2P$). The bottom panels shows the same diagrams for the secondary eclipse delay.

Several strong periodic signals are present in the eclipse timings, all of which arise from the rapid pulsations of the sdB star and inadequate emulation of the integration time of the observations. The latter issue, which we refer to as a ‘chunking’ problem, stems from the finite sampling time of each *Kepler* point, which distorts the light curve (see Kipping 2010). Even though we attempted to avoid the effects of chunking by taking integration into account in our model template, small mismatches in the way our model and data were binned remain. The same problem in accounting for chunking was encountered by Kipping & Bakos (2011). The effects of the sdB pulsations on the eclipse timings are even more pronounced. Although none of the 55 pulsational frequencies detected by Ø10 has an amplitude greater than 0.05%, the *Kepler* data are so precise these small oscillations also introduce noticeable asymmetries into the eclipse profiles. The phasing of the distortions changes from cycle to cycle, pulling around the best-fitting centroid values on timescales related to the beating of the pulsations with the orbital period. In some cases, such as the $f=0.26 \text{ d}^{-1}$ signal, the peak-to-peak amplitude about the mean approaches several seconds.

To model the influence of pulsations and chunking on the eclipse timings, we constructed a fake, noiseless light curve using our BINARY MAKER 3.0 template with the same sampling and integration as the Q5/Q6 *Kepler* data. We included all of the known pulsations to the light curve, using the frequencies and amplitudes given in Table D1 of Ø10. Their phases were defined randomly since they were not provided by Ø10. We forced the secondary eclipse to occur exactly halfway between primary eclipses to determine whether the pulsations affect our measurement of the mean time delay. A second model light curve, identical to the first sans pulsations, was also constructed. We repeated the entire analysis procedure for the synthesized data; Figure 5 shows the resulting eclipse measurements and their amplitude spectra.

The influence of pulsations and finite sampling on the eclipse timings is drastic; the O-C diagram FTs reveal a large number of periodicities, none of which represents a ‘real’ signal in the data. A comparison of Figures 4 and 5 shows that each frequency in the observed timings corresponds to one of the spurious signals generated by adding the finite sampling and the sdB pulsations to our model light curve. Most of the signals arise from the stellar pulsations. Their presence, however, does not offset the mean delay measured for the secondary eclipse. The best-fitting Gaussian to the distribution of Δt_{SE} values, shown in the top panel of Figure 6, is centered at 0.03 ± 0.11 s, consistent with the modeled offset of zero. Luckily, the spurious timing oscillations are so rapid compared to the run length that we sampled an adequate number of cycles during Q5/Q6 that their mean is very nearly zero. For this reason, the uncertainties of the pulsation phases do not affect our results. If we repeat the above

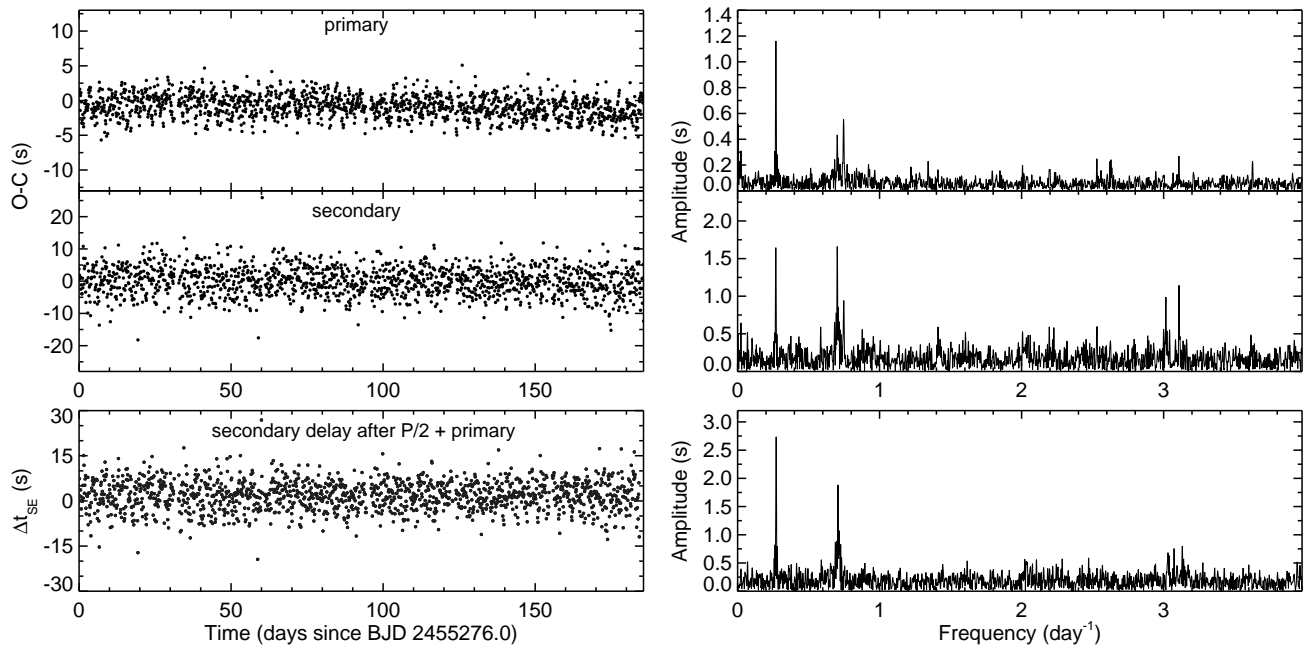


FIG. 4.— *Top panels:* O-C diagrams (left) constructed from primary and secondary eclipse timings in Q5/Q6 and their respective Fourier transforms (right). Several periodic signals are visible in the eclipse timings with periods ranging from 0.25-3.7 days *Bottom panels:* Time delay of the secondary eclipse with respect to one half period after the primary eclipse (left) and its FT (right). Some of the same periodicities detected in the O-C diagrams are also present here.

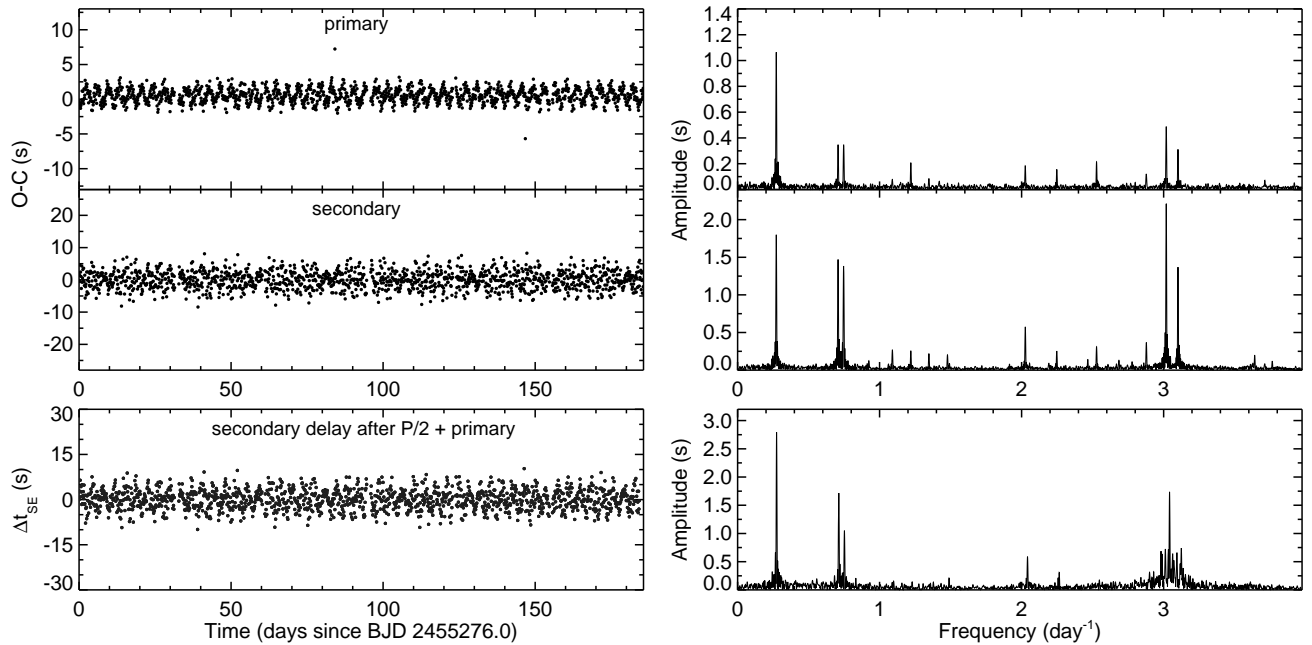


FIG. 5.— Same as Figure 4, but for a synthesized binary light curve with all 55 pulsation frequencies from $\text{O}10$ added. The pulsations and finite sampling skew the eclipse profiles in a periodic fashion that gives rise to apparent oscillations in the arrival times of the eclipses. Note the alignment between these signals and those in Figure 4. No noise was added to the model light curve.

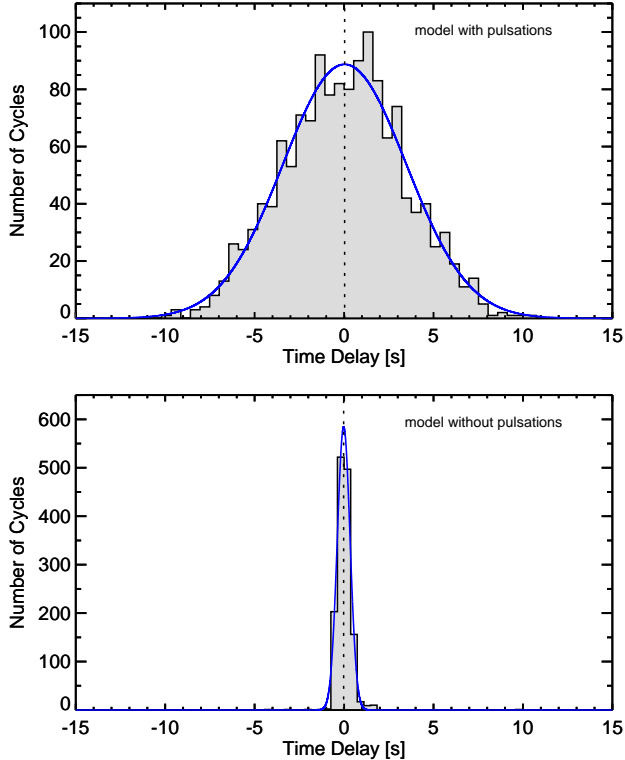


FIG. 6.— Same as Figure 3, but for a noiseless, synthesized light curve with (top) and without (bottom) pulsations. The model was constructed with secondary eclipses occurring exactly halfway between primary eclipses. The presence of the sdB’s pulsations inflates the distribution of eclipse measurements by a factor of 9.7 but does not change the mean significantly.

analysis using the model without pulsations, the distribution is significantly narrower, as seen in the bottom panel of Figure 6. The best-fitting Gaussian centroid in this case is -0.023 ± 0.003 s. Although the pulsations don’t significantly affect the mean time delay measured, they do inflate the distribution width by a factor of 9.7.

Our light-curve synthesis exercise tells us the centroid of the best-fitting Gaussian to the observed Δt_{SE} distribution in Figure 3 reflects the true offset in the system, even though the distribution of measurements is inflated significantly by the pulsations. Thus, we report a time delay of $\Delta t_{\text{SE}} = 2.06 \pm 0.12$ s for the secondary eclipse, as measured from the mid point between primary eclipses. Note that this offset remains constant from Q0 to Q5/Q6 (bottom panel of Figure 2), in spite of the seven-second phase shift from the period change.

4. DERIVATION OF THE MASSES

We can derive the masses of the hot subdwarf (M_{sd}) and cool companion (M_c) from the eclipse timings using the equations presented by Kaplan (2010). In a binary system with exactly circular orbits and unequal masses, secondary eclipses will not occur exactly 1/2 period after the primary eclipses due to the extra light-travel time (LTT) required. This Rømer delay (Δt_{LTT}) is given by

$$\Delta t_{\text{LTT}} = \frac{PK_{\text{sd}}}{\pi c} \left(\frac{1}{q} - 1 \right) \quad (1)$$

where P is the orbital period, K_{sd} the sdB orbital veloc-

ity, q the mass ratio (M_c/M_{sd}). Small eccentricities will affect the relative timing of the primary and secondary eclipses through an additive⁵ term Δt_e defined by

$$\Delta t_e \simeq \frac{2Pe}{\pi} \cos \omega \quad (2)$$

where e is the eccentricity and ω the argument of periastron (Sterne 1940; Winn 2010; Kaplan 2010⁶). Thus, for small eccentricities, the total shift of the secondary eclipse with respect to 1/2 orbital period after the primary eclipse is

$$\Delta t_{\text{SE}} \simeq \Delta t_{\text{LTT}} + \Delta t_e \quad (3)$$

In §3, we found an average secondary eclipse time delay of about two seconds with respect to the mid-point between primary eclipses. This measurement represents Δt_{SE} in the above equation, and in order to use it to calculate the masses, the contribution from the eccentricity (Δt_e) must be identified. Surprisingly, an eccentricity of only $e = 0.0003$ could shift the secondary eclipse by the full amount we observe; to separate the Rømer delay out from the total measured delayed requires knowing the system’s eccentricity to a level of precision better than this. The radial velocity curve published by Ø10 only limits e to ~ 0.02 or smaller⁷. Theoretically, one could measure the eccentricity by looking for the apsidal motion predicted by general relativity and classical mechanics, which is straight-forward to calculate. The periastron advance (changing ω) induced by these effects would give rise to oscillations in the eclipse timings, and in particular Δt_{SE} , with known periods. The presence or absence of such a signal in the data allows one to place upper limits on the eccentricity. For typical eclipsing sdB+dM systems, unfortunately, the expected precessional periods are several decades, too long to be measured with the current dataset.

Without knowing the eccentricity to the required precision, we continue under the assumption of a circular orbit. Combining the observed 2.06-s delay with P and K_{sd} (from Ø10), we derive a mass ratio (via Eqn. 1) of $q = 0.2691 \pm 0.0018$. This result is independent of the orbital inclination angle. Upon assuming a particular inclination, we can also solve for the individual masses by combining Eqn. 1 with Kepler’s Third Law, as done by Kaplan (2010) in his Eqn. 7. He assumes a perfectly edge-on system in deriving this expression, and so it must be modified by a multiplicative term $(\sin i)^{-3}$ for our use. If we adopt the light curve modeling result $i=69.45 \pm 0.02$ deg from Ø10, we derive masses of $M_1=0.372 \pm 0.024 M_{\odot}$ and $M_2=0.1002 \pm 0.0065 M_{\odot}$. Additional orbital parameters calculated from the timing method are summarized in Table 3.

Our derived mass ratio does not agree with the light-curve modeling results of Ø10, from which we infer $q=0.244 \pm 0.008$; the disagreement in the masses themselves is even more pronounced. Their mass ratio predicts a time delay of 2.35 ± 0.10 s, which is 0.29 ± 0.16

⁵ Eqn. 1 should also be multiplied by an eccentricity term, but this addition changes Δt_{LTT} by less than 1% for $e < 0.1$. We ignore it here.

⁶ The Kaplan (2010) expression (his Eqn. 6) is missing a factor of 2.

⁷ as estimated from an F-test showing that $e > 0.02$ gives a significantly worse fit than a circular-orbit solution.

s longer than our result. This difference (significant at roughly 2σ), can easily be explained if the eccentricity is as small as $e = 0.00004 \pm 0.00002$! We cannot measure such a minuscule departure from the circular-orbit case using the currently-available data. Although non-zero e likely explains the disagreement, shortcomings in the light curve modeling might also be at play. Presumably, a revised light-curve analysis with q fixed at 0.2691 ± 0.0018 would result in a slightly different inclination. Unfortunately, the brief description of the light-curve modeling given in Ø10 does not allow us to predict a revised inclination with confidence. Our inferred masses are therefore provisional. We note, however, that in order to get an sdB mass equal to $0.48 M_{\odot}$ (Ø10’s derived value) using the observed P , Δt_{LTT} , and K_{sd} , the inclination would have to be 66.7 deg, in disagreement with the light curve modeling result. This discrepancy might be explained by a number of uncertainties associated with the light curve solution, including how to accurately model the M dwarf albedo and the *Kepler* bandpass. Their solution also depends greatly on the quoted value of $\log g$. Significant changes larger than their $1\text{-}\sigma$ error (0.009 dex) might come about from non-LTE modeling (versus their LTE solution), unaccounted-for rotational broadening of the H Balmer lines, and incomplete removal of the orbital velocities upon summation of the spectra for fitting. In light of some of these effects, Ø10 themselves stress that their model parameters are subject to systematic errors that might be larger than the statistical errors they cite.

5. CONCLUSIONS

Using three months of short-cadence *Kepler* photometry, we have shown that primary and secondary eclipse timings can help constrain the component masses in sdB+dM eclipsing binaries using the technique described by Kaplan (2010). The secondary eclipses of 2M 1938 arrive nearly two seconds after the halfway point between primary eclipses. Assuming a circular orbit, we are able to derive the mass ratio and individual component masses from this delay, the orbital period, the sdB velocity, and the inclination angle. Our total system mass and the mass ratio disagree with the results of Ø10. However, this difference may be reconciled if the system has an eccentricity no less than ~ 0.00004 , which is too small to be measured using the currently-available data. This work, and the concurrent study of KOI-74 by Bloemen et al. (2012), represent the first detections of secondary eclipse Rømer delays in compact binaries. The results of both studies, however, are fundamentally *inconclusive* at this time; until the eccentricities in these systems are determined to a precision of $\sim 10^{-5}$, it is impossible to separate out the Rømer effect contribution from the total observed time delay. An eccentricity-induced time delay can easily and naturally explain the apparent disagreement between the Rømer delay and binary light curve modeling solutions for both 2M 1938+4603 and KOI-74.

If the binary light curve modeling solution and derived mass ratio from Ø10 are accurate, the time delay we measure implies 2M 1938 has a non-circular orbit with eccentricity no smaller than $e \sim 0.00004$. Close sdB+dM binaries are generally expected to have circular orbits, as they are likely the products of CE evolution. Even if some level of eccentricity remains after their formation,

their circularization timescales were thought to be short enough for the orbits to circularize within the lifetime of the sdB, around 100 Myr (Tassoul 1988; Zahn 1977). Several phenomena might explain a small eccentricity in 2M 1938’s orbit. Some recent studies of sdB+dM systems (e.g., Pablo et al. 2012) show the synchronization timescales might be longer than the EHB lifetime. The system also might have been born (following the CE phase) with the M dwarf’s spin misaligned with the orbit, since in the wider pre-CE binary there was no reason for it to become aligned. Spin-orbit misalignment has been reported for the young eclipsing binary DI Her (Albrecht et al. 2009). The resultant torques will give rise to a time-varying eccentricity, apsidal motion, precession of the orbital plane, and spin precession. (In this case the misaligned figure of the M dwarf would probably vitiate some of the assumptions of the light-curve model used by Ø10.) A third body orbiting outside the 3.0 h binary would perturb any initially circular orbit, resulting in orbital eccentricity. If the third-body orbit were not coplanar with the inner binary, one would expect to observe precession of the inner binary’s orbital plane as well. Any eccentricity will be damped out, at the expense of orbital energy, so another prediction is that the orbital period should be decreasing with time (as observed, although a longer timebase is needed to be sure that this is a truly secular phenomenon, rather than periodic or quasi-periodic). Eggleton (2006) discusses these processes and their associated amplitudes and timescales extensively. Random convective motions in the M dwarf could also lead to an eccentric orbit, since they induce fluctuations in the exterior gravitational field (Phinney 1992; Lanza & Rodonò 2001).

Due to strong irradiation, we expect some level of H-alpha emission from the M dwarf. If such a feature is detected and the eccentricity of the system is eventually determined to adequate precision, 2M 1938 will be unique among binaries in that the individual masses can be computed using at least four different techniques: double-lined spectroscopic binary analyses, asteroseismology, eclipsing binary light curve modeling, and eclipse timing monitoring. Comparisons of these results will help constrain the underlying physics in the light-curve modeling and asteroseismic codes.

This material is based upon work supported by the National Science Foundation under Grant No. AST-0908642. We are grateful to an anonymous referee for particularly helpful comments and suggestions that greatly improved this manuscript. The data presented in this paper were obtained from the Multimission Archive at the Space Telescope Science Institute (MAST). STScI is operated by the Association of Universities for Research in Astronomy, Inc., under NASA contract NAS5-26555. Support for MAST for non-HST data is provided by the NASA Office of Space Science via grant NNX09AF08G and by other grants and contracts. This paper includes data collected by the *Kepler* mission. Funding for the *Kepler* mission is provided by the NASA Science Mission directorate.

TABLE 3
SYSTEM PARAMETERS

Param	Value	Error	Unit	Comments
P	3.018 366 023	$\pm 0.000\,000\,048$	hrs	measured from <i>Kepler</i> Q0+Q5+Q6 primary minima at start of Q6
\dot{P}	-1.23	± 0.07	$10^{-10} \text{ s s}^{-1}$	measured from <i>Kepler</i> Q0+Q5+Q6 primary minima
K_{sd}	65.7	± 0.6	km s^{-1}	measured by Østensen et al. (2010)
i	69.45	± 0.02	deg	calculated by Østensen et al. (2010)
Δt_{SE}	2.06	± 0.12	s	measured from <i>Kepler</i> Q0+Q5+Q6 (from Gaussian fit to distribution)
q	0.2691 ^a	± 0.0018	-	calculated from Δt_{SE} , P , K_{sd}
M_{sd}	0.372 ^a	± 0.024	M_{\odot}	calculated from Δt_{SE} , P , K_{sd} , $\sin i$
M_{c}	0.1001 ^a	± 0.0065	M_{\odot}	calculated from Δt_{SE} , P , K_{sd} , $\sin i$
a	0.823 ^a	± 0.015	R_{\odot}	calculated from P , K_{sd} , $M_{\text{sd}}+M_{\text{c}}$
R_{sd}	0.196 ^a	± 0.049	R_{\odot}	estimated using $\log g$ and M_{sd}
K_{c}	244.2 ^a	± 2.8	km s^{-1}	estimated using q and K_{sd}

^aassumes a circular orbit.

REFERENCES

- Albrecht, S., Reffert, S., Snellen, I. A. G., & Winn, J. N. 2009, *Nature*, 461, 373
- Bloemen, S., Marsh, T. R., Degroote, P., Østensen, R. H., Pápics, P. I., Aerts, C., Koester, D., Gänsicke, B. T., Breedt, E., Lombaert, R., Pyrzas, S., Copperwheat, C. M., Exter, K., Raskin, G., Van Winckel, H., Prins, S., Pessemier, W., Frémat, Y., Hensberge, H., Jorissen, A., & Van Eck, S. 2012, *MNRAS*, in press (arXiv:1202.5553)
- Clausen, D. R., Wade, R. A., Kopparapu, R. K., OShaughnessy, R. 2012, *ApJ*, 746, 186
- Eggleton, P. 2006, *Evolutionary Processes in Binary and Multiple Stars*, (Cambridge, UK: Cambridge University Press)
- For, B.-Q., Green, E. M., Fontaine, G., Drechsel, H., Shaw, J. S., Dittmann, J. A., Fay, A. G., Francoeur, M., Laird, J., Moriyama, E., Morris, M., Rodríguez-López, C., Sierchio, J. M., Story, S. M., Strom, A., Wang, C., Adams, S. M., Bolin, D. E., Eskew, M., & Chayer, P. 2010, *ApJ*, 708, 253
- Gilliland, R. L., Jenkins, J. M., Borucki, W. J., Bryson, S. T., Caldwell, D. A., Clarke, B. D., Dotson, J. L., Haas, M. R., Hall, J., Klaus, T., Koch, D., McCauliff, S., Quintana, E. V., Twicken, J. D., & van Cleve, J. E. 2010, *ApJ*, 713, L160
- Groot, P. J. 2012, *ApJ*, 745, 55
- Han, Z., Podsiadlowski, P., Maxted, P. F. L., & Marsh, T. R. 2003, *MNRAS*, 341, 669
- Han, Z., Podsiadlowski, P., Maxted, P. F. L., Marsh, T. R., & Ivanova, N. 2002, *MNRAS*, 336, 449
- Heber, U. 1986, *A&A*, 155, 33
- Kaplan, D. L. 2010, *ApJ*, 717, L108
- Kipping, D., & Bakos, G. 2011, *ApJ*, 733, 36
- Kipping, D. M. 2010, *MNRAS*, 408, 1758
- Lanza, A. F., & Rodonò, M. 2001, *A&A*, 376, 165
- Østensen, R. H., Green, E. M., Bloemen, S., Marsh, T. R., Laird, J. B., Morris, M., Moriyama, E., Oreiro, R., Reed, M. D., Kawaler, S. D., Aerts, C., Vučković, M., Degroote, P., Telting, J. H., Kjeldsen, H., Gilliland, R. L., Christensen-Dalsgaard, J., Borucki, W. J., & Koch, D. 2010, *MNRAS*, 408, L51 (Ø10)
- Pablo, H., Kawaler, S. D., Reed, M. D., Bloemen, S., Charpinet, S., Hu, H., Telting, J., Østensen, R. H., Baran, A. S., Green, E. M., Hermes, J. J., Barclay, T., O'Toole, S. J., Mullally, F., Kurtz, D. W., Christensen-Dalsgaard, J., Caldwell, D. A., Christiansen, J. L., & Kinemuchi, K. 2012, *MNRAS*, in press (arXiv: 1202.3649)
- Phinney, E. S. 1992, *Royal Society of London Philosophical Transactions Series A*, 341, 39
- Qian, S.-B., Zhu, L.-Y., Dai, Z.-B., Fernández-Lajús, E., Xiang, F.-Y., & He, J.-J. 2012, *ApJ*, 745, L23
- Shakura, N. I., & Postnov, K. A., 1987, *A&A*, 183, L21.
- Sterne, T. E. 1940, *Proc. National Acad. Sci.*, 26, 36
- Tassoul, J.-L. 1988, *ApJ*, 324, L71
- Winn, J. N. 2010, in *Exoplanets*, ed. S. Seager (Tucson, AZ: University of Arizona Press), 55
- Zahn, J.-P. 1977, *A&A*, 57, 383